Highly selective and sensitive detection of volatile organic compounds using long wavelength InAs-based quantum cascade lasers through quartz-enhanced photoacoustic spectroscopy Ⓕ

Special Collection: Volatile Organic Compounds and their Applications

Kumar Kinjalk Ⓘ ; Francesco Paciolla Ⓘ ; Bo Sun; Andrea Zifarelli Ⓘ ; Giansergio Menduni Ⓘ ; Marilena Giglio; Hongpeng Wu ✉ Ⓘ ; Lei Dong Ⓘ ; Diba Ayache; Davide Pinto Ⓘ ; Aurore Vicet Ⓘ ; Alexei Baranov Ⓘ ; Pietro Patimisco Ⓘ ; Angelo Sampaolo ✉ Ⓘ ; Vincenzo Spagnolo Ⓘ

Check for updates

View Online   Export Citation

Articles You May Be Interested In

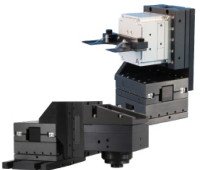Simultaneous dual-gas QEPAS detection based on a fundamental and overtone combined vibration of quartz tuning fork
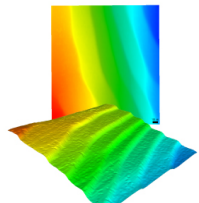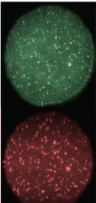
Appl. Phys. Lett. (March 2017)

Double antinode excited quartz-enhanced photoacoustic spectrophone

Appl. Phys. Lett. (January 2017)

Ultra-high sensitive acetylene detection using quartz-enhanced photoacoustic spectroscopy with a fiber amplified diode laser and a 30.72 kHz quartz tuning fork

Appl. Phys. Lett. (January 2017)

AIP Publishing

Highly selective and sensitive detection of volatile organic compounds using long wavelength InAs-based quantum cascade lasers through quartz-enhanced photoacoustic spectroscopy ⓕ

Kumar Kinjalk,[1,2] ⓘ Francesco Paciolla,[1] ⓘ Bo Sun,[1,3,4] Andrea Zifarelli,[1] ⓘ Giansergio Menduni,[1] ⓘ Marilena Giglio,[1] Hongpeng Wu,[3,4,a)] ⓘ Lei Dong,[3,4] ⓘ Diba Ayache,[2] Davide Pinto,[2] ⓘ Aurore Vicet,[2] ⓘ Alexei Baranov,[2] ⓘ Pietro Patimisco,[1,5] ⓘ Angelo Sampaolo,[1,5,a)] ⓘ and Vincenzo Spagnolo[1,3,5] ⓘ

AFFILIATIONS

[1]PolySense Lab, Dipartimento Interateneo di Fisica, University and Polytechnic of Bari, Via Amendola 173, Bari 70126, Italy
[2]IES, University of Montpellier, CNRS, 34095 Montpellier, France
[3]State Key Laboratory of Quantum Optics and Quantum Optics Devices, Institute of Laser Spectroscopy, Shanxi University, Taiyuan 030006, China
[4]Collaborative Innovation Center of Extreme Optics, Shanxi University, Taiyuan 030006, China
[5]PolySense Innovations srl, Via Amendola 173, Bari 70126, Italy

Note: This paper is part of the APR Special Topic on Volatile Organic Compounds and their Applications.
[a)]Authors to whom correspondence should be addressed: wuhp@sxu.edu.cn and angelo.sampaolo@poliba.it

ABSTRACT

The precise detection of volatile organic compounds plays a pivotal role in addressing environmental concerns, industrial safety, and medical diagnostics. The accurate identification and quantification of these compounds because of their ubiquity and potential health hazards has fueled the development of advanced sensing technologies. This work presents a sensing system in the realm of long-wavelength infrared spectroscopy for achieving enhanced selectivity and sensitivity of benzene, toluene, and propane detection through quartz-enhanced photoacoustic spectroscopy. High-resolution gas spectroscopy is made possible by the use of specially designed InAs/AlSb-based quantum cascade lasers, emitting in the wavelength range 13–15 μm, and quartz tuning forks. The sensor system, characterized by its robustness and precision, demonstrates exceptional capabilities in benzene, toluene, and propane detection. The system's capacity for practical applications in environmental monitoring and medical diagnostics is demonstrated by its ability to distinguish these volatile organic compounds with a minimum detection limit of 113 ppb, 3 ppb, and 3 ppm for toluene, benzene, and propane at an integration time of 10 s, even in complex gas matrices. This work advances gas sensing technology while also offering insightful information on spectral interferences, a persistent problem in the field. The results usher in a new era of sophisticated and reliable gas sensing techniques meeting the growing demand for precise volatile organic compounds detectors for environmental monitoring purposes.

INTRODUCTION

The need for accurate detection and quantification of volatile organic compounds (VOCs) such as hydrocarbons and BTEX (benzene, toluene, ethylbenzene, and xylene) has finally gained, during the last decade, the deserved level of attention within the environmental research community due to their high level of volatilization and toxicity. The exact identification of such compounds is crucial for monitoring air quality, identifying their origins, and evaluating possible health and environmental hazards because of their widespread production/use in industrial processes, transportation, and a variety of other areas.

BTEX have been identified as significant contributors to air pollution with detrimental effects on human health. The International Agency for Research on Cancer (IARC) and the United States Environmental Protection Agency (EPA) have both identified benzene

as a human carcinogen.[1,2] Leukemia, neurological diseases, and respiratory illnesses have all been related to long-term exposure to benzene.[3] Toluene, ethylbenzene, and xylene also provoke health problems due to their ability to contribute to the development of ground-level ozone[4] and smog, as well as their effects on the central nervous and respiratory system.[5,6] Propane on the other hand is generally considered safe.[7] However, its detection plays a crucial role in safe handling, storage, and usage of petroleum and natural gas. In industrial environments, accurate detection of propane is critical for preventing leaks, ensuring compliance with safety protocols, and optimizing fuel usage.

Therefore, the widespread application and potential hazards of these VOCs necessitate highly specific and sensitive detection methods. Moreover, in the field of medical diagnostics, an increasing number of studies has demonstrated the presence of abnormally elevated levels of these VOCs in exhaled breath as an indicator of certain diseases.[8–11] In the case of BTEXs, they can be found in exhaled breath mainly as exogenous biomarkers, most of the times in smokers and in individuals who have been exposed to BTEX anomalous concentrations in the environment. Hence, portable, sensitive, and selective breath sensors could potentially serve as noninvasive early diagnostic tools for point-of-care mass screening.

BTEX analysis has conventionally relied on established techniques, such as the combination of gas chromatography and mass spectrometry,[12,13] which have been widely regarded as the gold standard. The utilization of such techniques provides a notable degree of accuracy and sensitivity, facilitating precise measurement and differentiation of distinct BTEX constituents. Notwithstanding their efficacy, these methods tend to be slow, demand proficient personnel, and entail analysis in a laboratory setting, thereby rendering them less appropriate for expeditious on-site monitoring. Lately, to address these issues, various sensor types, including, but not limited to, electrochemical[14] and solid-state,[15] have been developed. These sensors offer improved detection sensitivity, selectivity, speed, portability, and ease of use. Nevertheless, stability, lifetime, and performances of these sensors are strongly affected by environmental conditions, such as temperature and humidity levels.

In this context, optical sensors have been identified as a viable solution for trace gas detection due to their capability to provide high sensitivity and selectivity by exploiting laser excitation of infrared molecular transitions. Optical sensors offer sophisticated functionalities for accurate and dependable gas analysis, relying on direct or indirect absorption techniques and taking advantages from the unique features of the laser devices in terms of narrow spectral bandwidth and high-power continuous wave operation.[16] Several works reported on infrared sensors to exploit the $3.3\,\mu m$ absorption range of benzene through techniques such as cavity-enhanced spectroscopy[17] and multi-pass absorption sensing via difference frequency generation.[18] Additionally, the ν_{14} band at $1023\,cm^{-1}$ has been investigated using tunable diode laser spectroscopy by employing a multi-pass Herriott cell with a path length of $472\,cm$.[19]

However, these spectral regions are characterized by a low selectivity, due to the strong overlap of BTEX and lighter hydrocarbons, as they share the same class of molecular vibrations (C–H stretching around $3.3\,\mu m$ and C–H bending around $7.0\,\mu m$).[20,21] An alternative to these spectral ranges is represented by the region $12–15\,\mu m$, where intense and well-separated BTEX spectral features occur.

The spectroscopic scenario involving BTEX absorption bands and the most relevant atmospheric absorbers/potential interferents, such as water vapor and carbon dioxide, in the $12.1–15.4\,\mu m$ wavelength range is represented in Fig. 1.

The absorption coefficient was simulated separately for pure compounds just for comparing shape and potential overlap of the absorption bands, regardless of the realistic concentration ranges of specific applications. Water vapor absorption lines are almost completely absent in this range, or at least irrelevant, while CO_2 spectrum although present, exhibits sharp lines that can be perfectly discriminated from the other VOCs of interest by suitably choosing operating pressures and modulation depths in a wavelength modulation spectroscopic configuration.[22]

However, in the long-wavelength IR spectral region, the state-of-the-art for coherent light sources is meager. The lack of sources suitable for tunable diode laser absorption spectroscopy (TDLAS) above $12\,\mu m$ is due to fundamental performance limitations of long wavelength semiconductor lasers. Interband diode lasers could in principle operate only at cryogenic temperatures because of the strong nonradiative Auger recombination in the materials with a small bandgap. Interband lasers are currently not available at all in the considered spectral range. This problem can be overcome in sources employing intersubband transitions where the Auger processes are much weaker. However, the electron lifetime in the upper level of an intersubband lasing transition, the main parameter responsible for the quantum cascade laser (QCL) optical gain, quickly drops with increasing emission wavelength, and the lasers emitting above $10\,\mu m$ exhibit poor performance. For this reason, conventional long wavelength QCLs based on InP are unable to operate in the continuous wave regime close to room temperature. The intersubband optical gain depends on the electron effective mass m^* in the quantum wells as $m^{*-3/2}$, which makes materials with a small m^* very attractive for the development of long wavelength QCLs. In this work, we employed QCLs where the lasing transitions occur in InAs quantum wells. Due to the small electron effective mass, InAs-based QCLs exhibit higher optical gain compared
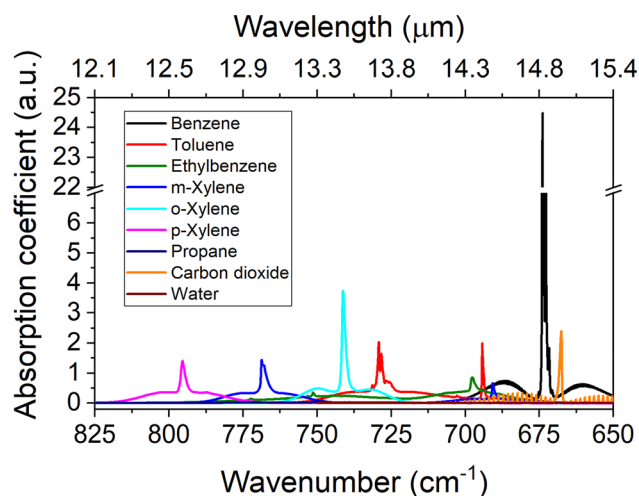

FIG. 1. Simulation of the absorption coefficient at atmospheric pressure of pure BTEX, water vapor, and carbon dioxide in the $12.1–15.4\,\mu m$ wavelength range, from HITRAN database.[21]

06 December 2024 08:15:39

with the InP-based counterparts[23] and demonstrated much better performance. Consecutive design adjustments allowed achieving room temperature continuous wave (CW) operation of such lasers at wavelengths up to 18 μm.[24] A detailed discussion on the design and characteristics of recent InAs-based long wavelength QCLs can be found in Ref. 25. For this study, the QCL structure was tailored to place the peak gain in the required spectral bands. The epitaxial wafers grown by molecular beam epitaxy were then processed into single frequency distributed feedback (DFB) lasers with a top metal grating[3] using electron beam lithography and dry and wet chemical etching. The devices exhibit good spectral purity with side mode suppression ratio (SMSR) > 20 dB, and tunability of ~2 cm^{-1}, enabling precise targeting of the absorption lines of benzene, toluene, and propane.

Recently, a tunable single-mode slot waveguide QCL array, emitting in the range 735.3–747.3 cm^{-1} (13.6 μm) has been demonstrated to be suitable for long wavelength spectroscopy of acetylene and o-xylene, implementing a hollow core fiber and a photovoltaic detector having a bandwidth optimized up to 10.6 μm.[26] The main limitation affecting direct absorption techniques, such as TDLAS[27] and cavity-enhanced absorption spectroscopy (CEAS),[28] mainly consists in the lack of commercially available long wavelength detectors suitable for sensing platform devoted to *in situ* and real time gas detection, and in the limited spectral bandwidth of high-quality optical components (for CEAS configurations in particular). The market of near- and mid-infrared photodetectors (PD) is dominated by amplified-PDs and thermoelectrically cooled photoconductive (PC) and photovoltaic (PV) detectors, respectively, which offer high responsivity but in a relatively narrow spectral range of operation below 10.6 μm. Beyond 11 μm, a narrow range of devices can be employed, mainly detectors based on photoconductive HgCdTe (MCT) technology, whose detectivity decreases by more than two orders of magnitude compared to those operating up to 10 μm.[29] Commercially available thermal PDs, such as pyroelectric detectors (PYDs) and Golay-cells (GC) can be exploited beyond 11 μm, with the drawbacks of (i) a relatively small noise equivalent power (NEP) and detection bandwidth for PYDs with respect to PV and PC and (ii) extremely low response times for GCs. Sophisticated setups requiring high performance in terms of NEP usually rely on commercial superconducting bolometers, which need liquid-helium cooling. Graphene has been demonstrated to be a promising material for infrared broadband photodetectors due to its gapless band structure,[30] but its low optical absorption limits drastically its responsivity and, in general, represents a novel technology far from reaching a commercial maturity.[31] From 2019, quartz tuning forks (QTFs) have been exploited as photodetectors in light-induced thermoelastic spectroscopy, exploiting the photo-thermo-elastic conversion of light within the structure of the mechanical resonator and proving a flat spectral response from ~1 to 10 μm.[32] Nevertheless, the effectiveness of this physical process up to 20 μm still needs to be demonstrated.

In the last 4 years, indirect spectroscopic approaches that can avoid the use of optical detectors, such as photoacoustic configurations, have been successfully demonstrated employing a QCL operating at 14.8 μm for benzene detection combined with (i) a standard 32 kHz tuning fork in a quartz-enhanced photoacoustic spectroscopy (QEPAS) system,[33] and with (ii) a cantilever-based photoacoustic sensor.[34] These advancements demonstrate the ongoing development and diversification of infrared sensing technologies, expanding the range of

applications and improving the detection capabilities in various spectral regions.

However, the detection of BTEX compounds, as well as the heavier alkanes like propane, butane, and pentane, presents unique challenges stemming from the potential spectral interferences among themselves or with other compounds. The presence of coexisting VOCs characterized by the same bonds can normally introduce spectral interferences especially in the spectral region where the fundamental bands of IR transitions lie, resulting in overlapping absorption features or distorted signals. For instance, while methane (C1) and ethane (C2) have been demonstrated to be easily separated and independently detected even at atmospheric pressure at 3.3 μm,[35,36] propane (C3) spectral features seem to be totally overlapping with C2 background absorption, making it difficult to discriminate and quantify C3 except through sophisticated multilinear or even multivariate approaches.[37] This issue of spectral interference should be eliminated at longer wavelength (13–15 μm) where BTEX and heavier hydrocarbons show distinct and isolated absorption features, like propane ν_{26} transition at 748 cm^{-1}.[38] Unfortunately, the lack of suitable laser sources has limited the development of these sensors at such long wavelengths.

In this landscape, the following study aims to demonstrating the effectiveness of an optical sensor with high sensitivity and selectivity for detecting two representative BTEXs (benzene and toluene) and heavy hydrocarbons, such as propane. The sensor is based on QEPAS technique and combines custom-designed quartz tuning forks with noncommercial long-wavelength QCLs emitting in the range 13–15 μm. With respect to standard QTFs employed so far, the lower frequency of the custom resonators helps in improving the energy relaxation efficiency, while the custom design and dimensions help in reducing the optical noise introduced by poor quality laser beams. Following a careful analysis of each VOC's absorption bands, the QCLs have been designed to operate at specific wavelengths, exciting the most suitable and intense absorption features for wavelength modulation detection. The design of the QCL structure used in this study has been extensively discussed in previous works.[39] These devices exhibit good spectral purity with side mode suppression ratio (SMSR) > 20 dB, and tunability of ~2 cm^{-1}, enabling precise targeting of the absorption lines associated with benzene, toluene, and propane. Using the developed sensing system, we have examined and confirmed the absence of both spectral and non-spectral interference among BTEX. Moreover, we have also verified the selectivity of propane detection within gas matrices rich in C1 and C2. In this case as well, non-spectral cross sensitivities have been shown to be insignificant.

This research work paves the way to the development of modular point-sensing QEPAS detectors, highly adaptable to the (i) excitation wavelength, (ii) quality of the laser beam, and (iii) composition of the gas matrix.

EXPERIMENTAL SETUP

The laser sources employed for this investigation consist in three InAs-based distributed feedback quantum cascade lasers designed to emit at wavelengths resonant with absorption bands of toluene (QCL$_T$ $\lambda = 13.71$ μm), benzene (QCL$_B$ $\lambda = 14.85$ μm), and propane (QCL$_P$ $\lambda = 13.36$ μm). The design, growth, and fabrication of these devices were carried out at IES, University of Montpellier. The fabricated DFB QCLs are mounted on aluminum nitride (ALN) heatsink, collimated, and packaged in a customized enclosure equipped with a PT100[40]

temperature sensor and a Peltier cooling element. External water cooling is also available in the enclosure to aid in extracting heat generated by the Peltier element. The operating temperature range for these QCLs in a CW regime extends from $-20\,°C$ to close to room temperature. In this experiment, specific operating temperatures have been selected to target and allow an efficient exploitation of the identified spectral fingerprints: -10, -5, and $3\,°C$ for QCL_T, QCL_B, and QCL_P, respectively.

Figure 2(a) illustrates the optical power vs current and voltage vs current characteristics of QCL_T, QCL_B, and QCL_P at the specified temperatures. The optical power reaches 11, 4, and 3 mW, respectively.

Figure 2(b)–2(d) displays the absorption coefficient for toluene, benzene, and propane at atmospheric pressure as a function of wavenumber (solid lines), as obtained from the NIST [Figs. 2(b) and 2(c)][41] and HITRAN [Fig. 2(d)] database. Additionally, datapoints depict the wavelength tuning range of the devices as a function of the injection current, at the selected operating temperatures. As reported in the introduction section, these absorption features are related to different molecular vibrations. The benzene and toluene (BT) bands correspond to aryl C–H out-of-plane bending, while the propane rotational structure refers to C-type CH_2-rocking fundamental mode.[38,42] BT bands are both more separated and more intense with respect to the $3–4\,\mu m$ spectral window where aryl C–D stretching is mostly involved, while

propane shows absorption coefficients $\sim$50 times stronger at 3369 nm, but an almost total overlap with lighter hydrocarbons.

The QEPAS sensing system with the possibility to interchange the three DFB QCLs is schematically depicted in Fig. 3. The sensor head, the gas line, and the electronic components used to drive the QCLs and acquire data are included in the schematic.

The sensor head includes an acoustic detection module (ADM) equipped with two germanium optical windows, inlet and outlet connectors to regulate gas flow, and houses a spectrophone composed of a T-shaped QTF acoustically coupled with a pair of resonator tubes, composing a spectrophone. The dimensions of the T-shaped QTF are documented in Ref. 43. The millimeter-size resonator tubes (mRes) are positioned 2 mm below the top of the QTF, perpendicular to its plane, and separated by a gap measuring 0.2 mm. The mRes are 12.4 mm long and have an internal diameter of 1.59 mm and an external diameter of 1.83 mm. The T-shaped custom resonator was selected because of three main reasons: (i) its nominal resonance frequency, i.e., 12.5 kHz, (ii) the prongs' gap of 0.8 mm, and (iii) the experimental value of the SNR enhancement provided by the spectrophone with respect to the bare QTF. In fact, fundamental resonance modes in the range 12–15 kHz were demonstrated to be the best trade-off between QTF quality factors and compatibility of the resonance frequencies with the typical energy relaxation times of molecules in the range
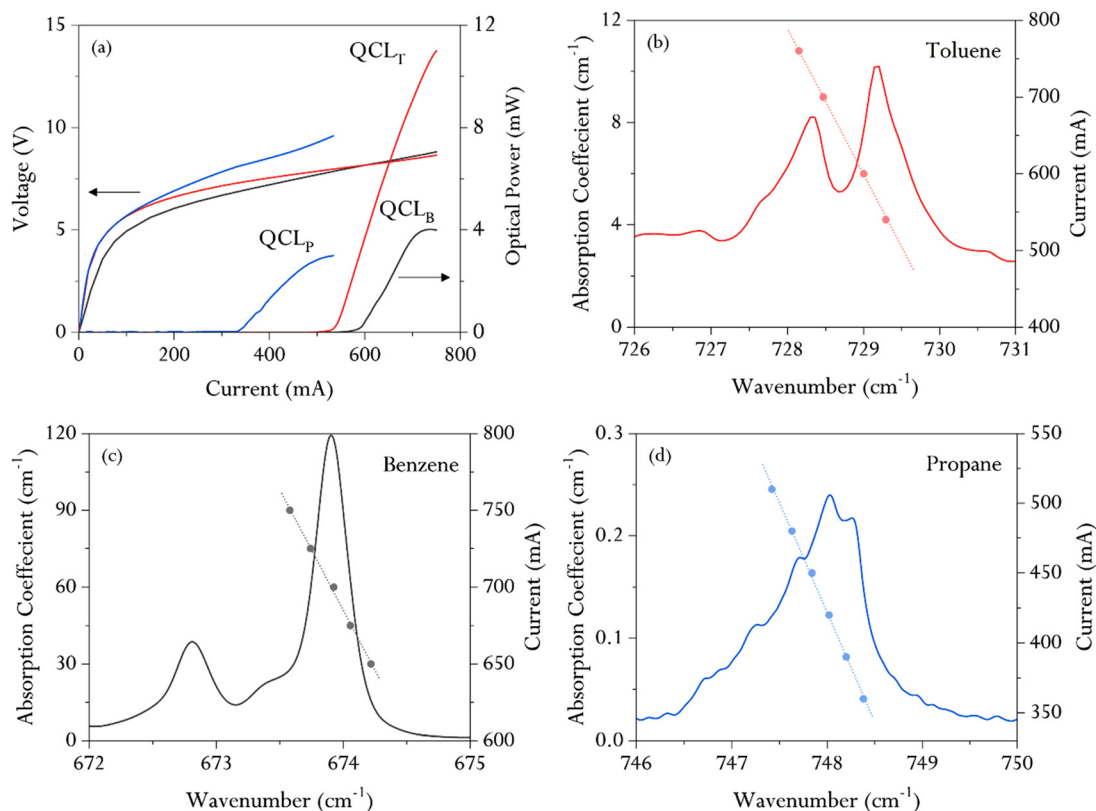

FIG. 2. (a) Optical power vs current and voltage vs current characteristics of QCL_T (red curves), QCL_B (black curves), and QCL_P (blue curves) operating at -10, -5, and $3\,°C$, respectively. (b)–(d) Solid lines represent the simulation of the absorption coefficient for pure toluene, benzene, and propane at atmospheric pressure. The spectra of the absorption coefficient of toluene and benzene are obtained from the NIST database, while the propane spectrum is obtained from the HITRAN database. Dotted lines and solid symbols mark the QCL wavelength tuning ranges as a function of the QCLs' injection current.
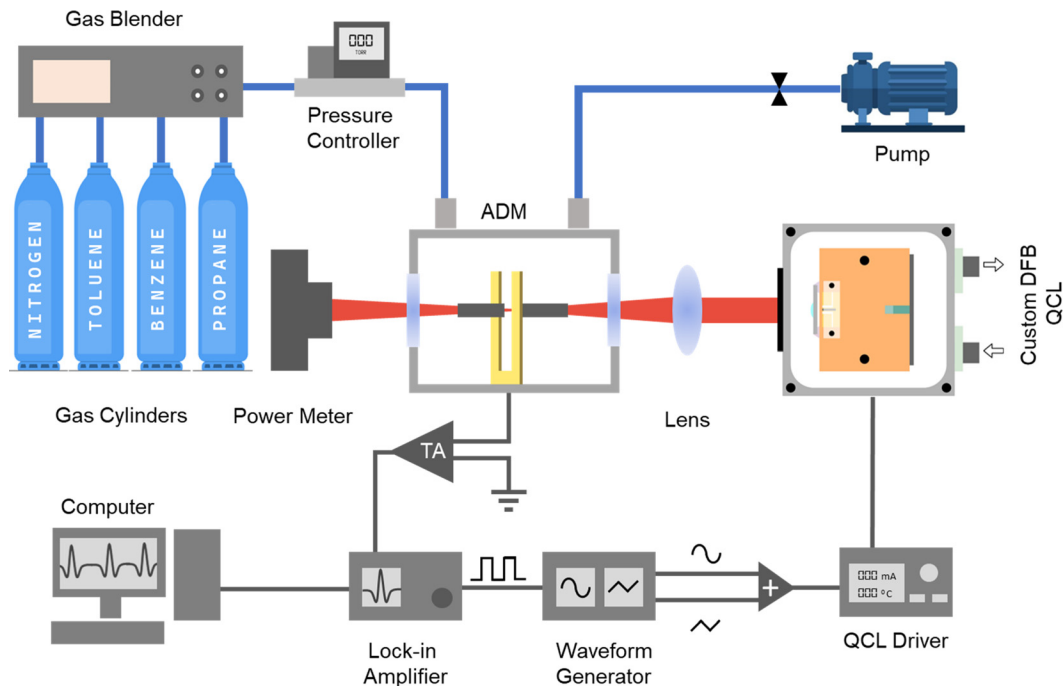
FIG. 3. The schematic diagram of the QEPAS sensor system employing custom InAs-based long wavelength DFB QCL (distributed feedback quantum cascade laser). ADM: acoustic detection module and TA: transimpedance amplifier.

100–760 Torr.[44] Moreover, the experimental SNR enhancement of ~60 for the T-shaped QTF is the largest demonstrated so far.[45] The larger prongs' spacing with respect to the 0.3 mm of the standard QTF is particularly useful for accommodating large beam waist of long wavelengths as well as poor quality beams.[45] The resonance frequency and quality factor of the fundamental in-plane flexural mode for the specific resonator employed in this work have been retrieved via inverse piezoelectric effect, i.e., by exciting the resonator with a sinusoidal voltage signal and performing a frequency sweep. Both resonance

curve and f, Q values as a function of pressure are plotted in Fig. 4. Under atmospheric pressure and in a mixture of pure N_2, the QTF exhibits a resonance frequency of $f_0 = 1\,245\,727$ Hz and a quality factor of $Q = 9296$.

Components of the gas line include certified gas cylinders, a gas blender, a pressure regulator, a needle valve, and a vacuum pump. With pure N_2 as the carrier gas, the gas blender (MCQ Instruments) is used to precisely control the flow rate of each individual gas channel and produce the desired gas mixture. An Alicat pressure controller/
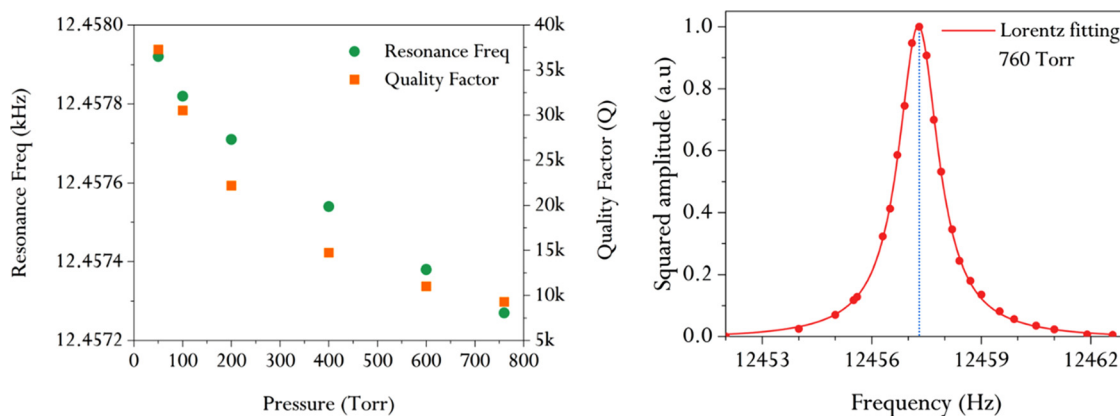

FIG. 4. (left) QTF resonance frequency (green circles) and quality factor (orange squares) as a function of pressure. (right) Resonance curve of the QTF at 760 Torr. The squared amplitude of the QTF signal is plotted as a function of the excitation frequency. The red circles represent acquired data, while the red curve is a fit of the data using a Lorentzian function. The blue dotted line indicates the resonance peak corresponding to the QTF frequency.

flow meter, in conjunction with a needle valve and a pump, is used to precisely regulate gas pressure and flow rate within the gas line. The gas flow rate is maintained at a constant value of 50 sccm, with a precision of 1% for the flow setpoint for every channel. To control the QCLs, a combined laser current driver and TEC controller (Thorlabs ITC4002QCL) is used. The current driver provides the necessary current to operate the QCLs and the TEC controls operation temperature. The collimated beam is focused between the prongs of the QTF, through Ge optical window and the resonator tubes, into the ADM, using a ZnSe plano–convex lens with a focal length of 50 mm having a 3–2 μm antireflection coating. The ADM is mounted on a five-axis stage to ensure precise alignment. Alignment is critical in preventing the laser beam tail from hitting the resonator tubes and/or the quartz tuning fork prongs, which can produce a non-zero background and negatively impact the sensor's detection sensitivity.[43] The alignment process is aided by an optical power meter (THORLABS PM100D).

To carry out QEPAS measurements, the wavelength modulation and 2f detection method is employed.[46] This involves applying a sinusoidal dither, which matches half of the QTF resonance frequency, to the QCL current driver. A transimpedance amplifier is then used to convert the resulting piezoelectric charge into an electrical signal. The transduced QTF signal is demodulated by a lock-in amplifier (MFIA 500 kHz Lock-in Amplifier, Zurich Instruments) at the QTF resonance frequency. A lock-in time constant of 100 ms is used in this process. The demodulated signal is then digitized and saved on a personal computer using a data acquisition board, with the sampling time set to three times the lock-in time constant.

SENSOR OPTIMIZATION, SENSITIVITY, AND MINIMUM DETECTION LIMIT

In QEPAS, the optimization of gas pressure and modulation depth is of critical importance to enhance the sensitivity of the QEPAS system. When dealing with purely Lorentzian and isolated optical transitions, the operating pressure optimization has the main goal of finding a trade-off between the increase in the QEPAS signal as the target

molecules increases (and so the pressure), and the QTF's quality factor deterioration due to increasing of the working pressure. Once the optimum pressure maximizing the QEPAS signal is identified, the optimum modulation depth for a purely Lorentzian and isolated feature is mainly determined by its linewidth.[46] In the case of broadband absorption features with the presence of interferents, the identification of the optimum working pressure becomes more a matter of trade-off between[29] maximizing the QEPAS signal and the spectral selectivity, posing the issue of an accurate reconstruction of the spectral fingerprint of the target features. For example, at a fixed operating pressure, the effect of overmodulation may provide a generally intense signal spectrum, but with the drawback of being composed of less-characteristic features for signal discrimination with respect to potential interferents.[22,23] In this perspective, it is thus crucial to preserve the derivative shape of the absorption profile as well as to prevent the modulation depth from exciting nearby absorption features of potential interferents. In fact, the experimental determination of the best operating conditions in terms of pressure and QCL current modulation depth aims at achieving the right balance between signal enhancement and spectral distinctiveness of the absorption features for each target molecule.[22]

Figures 5–7 (left) show the normalized QEPAS peak signals as a function of modulation depth at different pressures for certified concentrations of toluene (150 ppm in N_2), benzene (100 ppm in N_2), and propane (1000 ppm in N_2) by interchanging QCL_T, QCL_B, and QCL_P, respectively, in the QEPAS system depicted in Fig. 3. The pressure ranges of investigation are different from analyte to analyte. Pressures lower than 50 Torr for benzene and toluene and 200 Torr for propane were not considered because the QEPAS signal was too low in the overall investigated range of modulation depth. It is evident from Figs. 5–7 (left) that as the pressure increases, there is a corresponding rise in the QEPAS peak signal. However, as the pressure and the modulation depth increase, the target feature experiences a rising distortion as well as the whole spectrum, with the result of deteriorating its spectral specificity. In fact, the reference absorption feature for toluene
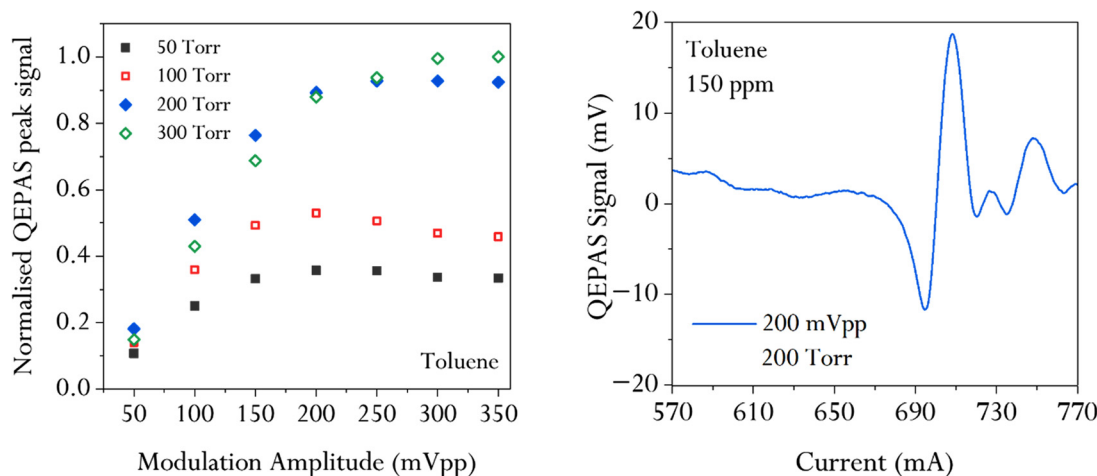

FIG. 5. (left) Normalized QEPAS peak signal of toluene plotted against the laser peak-to-peak modulation amplitude at various pressures. (right) QEPAS signal of 150 ppm of toluene obtained by sweeping the laser injection current within the QCL_T tuning range at optimal working conditions, i.e., 200 mV peak-to-peak laser current modulation amplitude and 200 Torr.
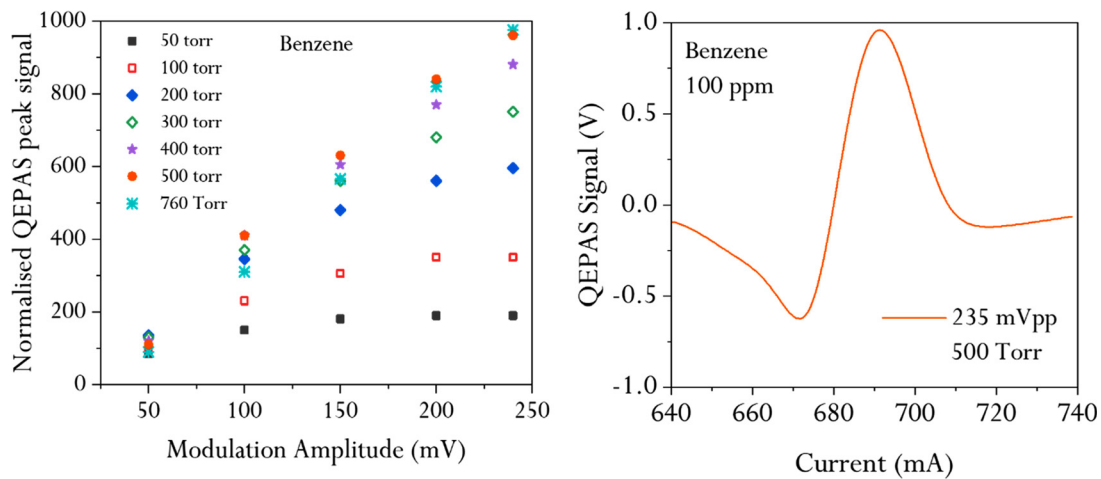
FIG. 6. (left) Normalized QEPAS peak signal of benzene plotted against the laser peak-to-peak modulation amplitude at various pressures. (right) QEPAS signal of 100 ppm of benzene obtained by sweeping the laser injection current within the QCL$_B$ tuning range at optimal working conditions, i.e., 235 mV peak-to-peak laser current modulation amplitude and 500 Torr.

resulted already heavily distorted at pressures higher than 300 Torr: for this reason, the investigation was restricted in the range 50–300 Torr. Based on these observations, the optimum pressure and modulation depth were selected, considering the maximum signal amplitude recorded for the most intense feature of each analyte's spectrum but always preserving the characteristic shape of the spectra for selectivity issues. For toluene, the optimal pressure was determined to be 200 Torr, with a corresponding optimal modulation depth of 200 mVpp. For benzene, the optimal pressure was found to be 500 Torr, with an optimal modulation depth of 235 mVpp. Finally, for propane, the optimal pressure was determined to be 400 Torr, accompanied by an optimum modulation depth of 300 mVpp. The QEPAS spectrum showcasing the

absorption peaks for each gas at respective identified optimum working conditions are presented in Figs. 5–7 (right) for toluene, benzene, and propane, respectively.

To determine the sensitivity for each gas species, a calibration process was conducted by acquiring spectral scans at different gas target concentrations obtained by diluting the certified gas mixture with humidified nitrogen (N_2), as shown in Figs. 8–10 (left). The peak value of the most intense absorption feature for each analyte was extracted and plotted as a function of the corresponding molecule concentration. These data have been fitted by a linear interpolation, showing an excellent linearity for each molecule, as depicted in Figs. 8–10 (right). These calibrations allowed determining the sensitivity levels through the relative slopes, resulting in 0.12, 8.9, and 0.003 mV/ppm for toluene,
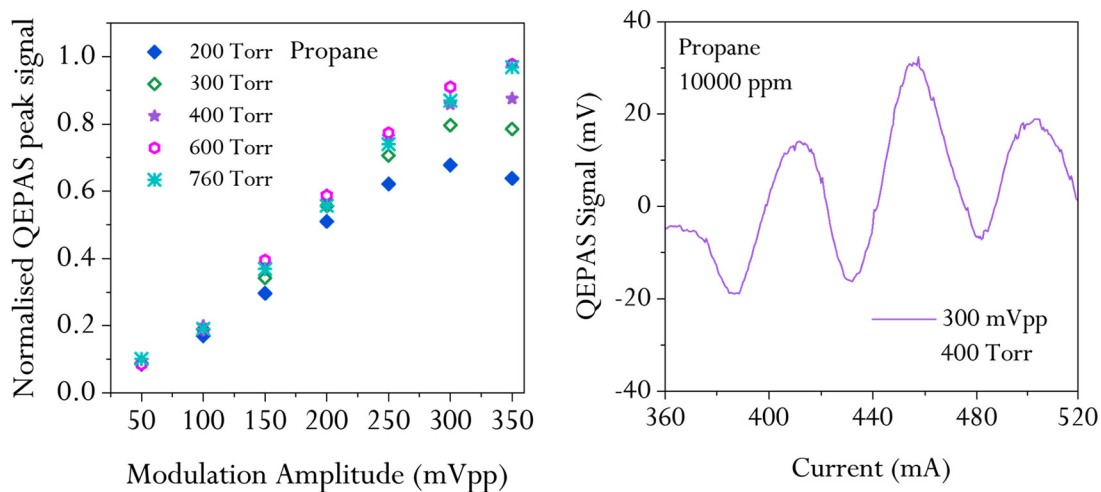

FIG. 7. (left) Normalized QEPAS peak signal of propane plotted against the laser peak-to-peak modulation amplitude at various pressures. (right) QEPAS signal of 10 000 ppm of propane obtained by sweeping the laser injection current within the QCL$_P$ tuning range at optimal working conditions, i.e., 300 mV peak-to-peak laser current modulation amplitude and 400 Torr.
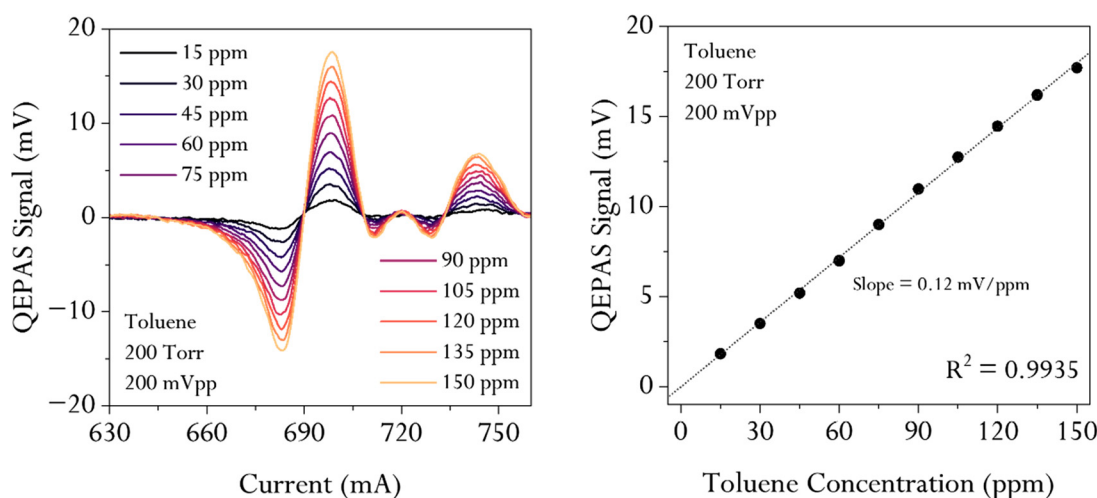
FIG. 8. (left) QEPAS signal of toluene obtained by sweeping the laser injection current within the QCL_T tuning range at optimal working conditions, i.e., 200 mV peak-to-peak laser current modulation amplitude and 200 Torr. (right) Peaks of most intense feature plotted against toluene concentration (black circles). The slope and R-squared values of the linear fit (black dotted line) are reported.

benzene, and propane detection, respectively. The noise level (0.07, 0.15, and 0.07 mV for toluene, benzene, and propane, respectively) was calculated as the standard deviation (1σ) of the sensor response when there is no optical absorption, typically achieved by flowing pure nitrogen through the QEPAS cell.

To estimate the achievable minimum detection limit (MDL) as a function of the lock-in integration time, an Allan–Werle deviation analysis was performed on a noise acquisition of 2.5 h. The Allan–Werle deviation analysis is shown in Fig. 11. The sensor exhibited an MDL of 375 ppb, 13 ppb, and 15 ppm for toluene, benzene, and propane, respectively, at a lock-in integration time of 0.1 s. By increasing the integration time, it is possible to enhance the sensitivity and thus improve the detection limit of the sensing system. The MDLs

corresponding to a 10 s integration time are marked in Fig. 11. The Allan deviation analysis demonstrates that for integration times less than 100 s (toluene and propane) and 60 s (benzene), the noise level closely follows a $1/\sqrt{t}$ dependence. This observation suggests that the dominant source of noise in QEPAS is the thermal noise in the quartz tuning fork (QTF). For longer integration times, sensitivity deteriorates. This behavior can be primarily attributed to the occurrence of other long-term effects, such as laser and mechanical instabilities, as well as slow temperature drifts.

SELECTIVITY ANALYSIS

To ensure accuracy and reliability in detecting specific gases, the importance of selectivity in sensors cannot be overstated. High
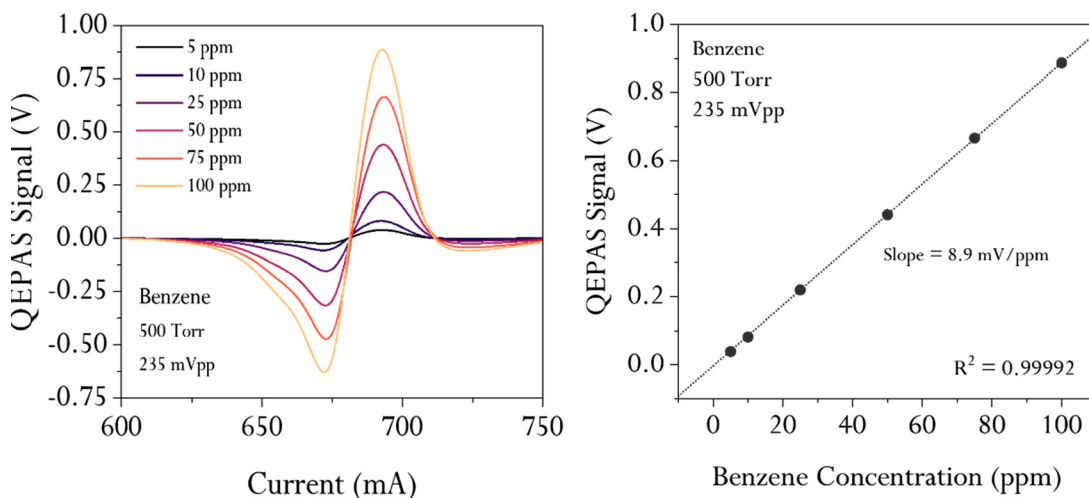

FIG. 9. (left) QEPAS signal of benzene obtained by sweeping the laser injection current within the QCL_B tuning range at optimal working conditions, i.e., 235 mV peak-to-peak laser current modulation amplitude and 500 Torr. (right) Peaks of most intense feature plotted against benzene concentration (black circles). The slope and R-squared values of the linear fit (black dotted line) are reported.
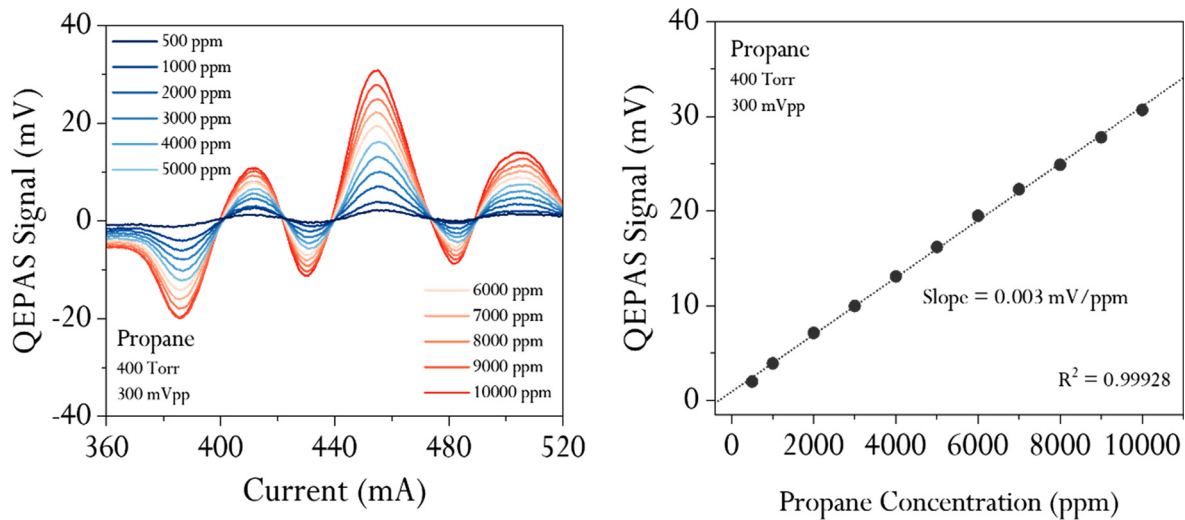
FIG. 10. (left) QEPAS spectra of propane obtained by sweeping the laser injection current within the QCL_P tuning range at optimal working conditions, i.e., 300 mV peak-to-peak laser current modulation amplitude and 400 Torr. (right) Peaks of most intense feature plotted against propane concentration (black circles). The slope and R-squared values of the linear fit (black dotted line) are reported.
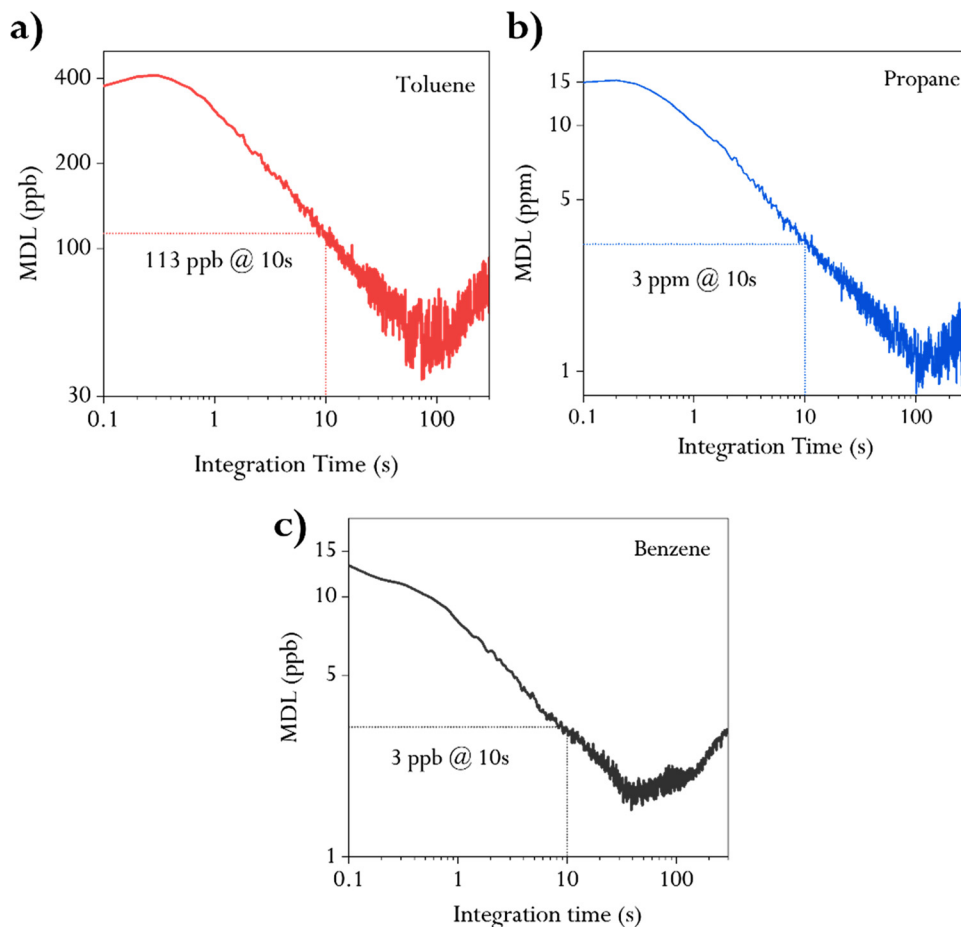

FIG. 11. (a)−(c) Allan–Werle deviation analysis of toluene, benzene, and propane, respectively, reporting the minimum detection limit as a function of lock-in integration time. The minimum detection limit achieved for an integration time of 10 s is marked for each gas species.
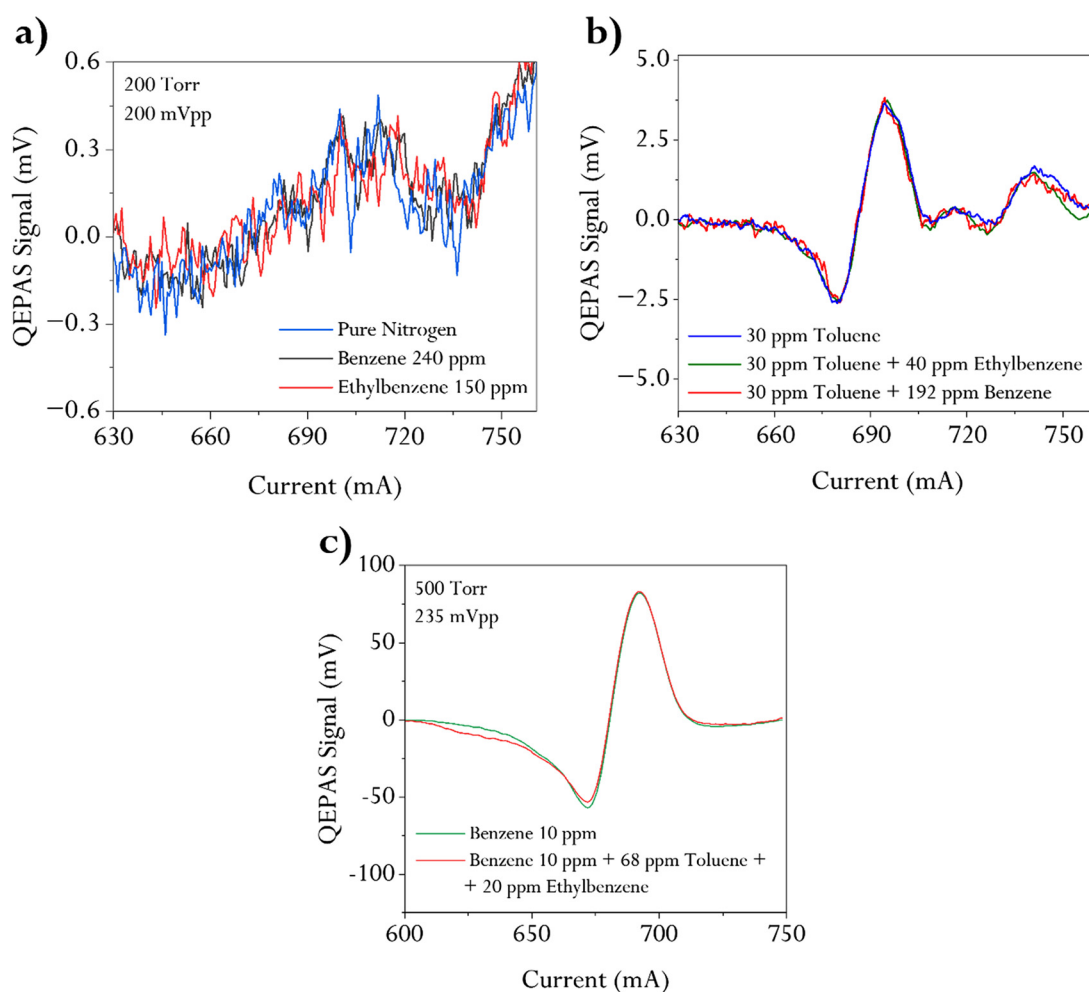
06 December 2024 08:15:39

FIG. 12. (a) Comparison between the QEPAS signal obtained for 240 ppm of benzene in nitrogen (black line), for 150 ppm of ethylbenzene in nitrogen (red line), and for pure nitrogen (blue line) obtained by sweeping the laser injection current within the QCL_T tuning range at 200 mV peak-to-peak laser current modulation amplitude and 200 Torr. (b) Comparison between the QEPAS signals of 30 ppm of toluene in nitrogen (blue line) and two mixtures: 30 ppm of toluene mixed with 40 ppm ethylbenzene in nitrogen (green line) and 30 ppm toluene mixed with 192 ppm of benzene in nitrogen (red line) obtained in the same experimental conditions as in (a). (c) Comparison between the QEPAS signals of 10 ppm of benzene in nitrogen (green line) and a mixture of 10 ppm of benzene, 68 ppm of toluene, and 20 ppm of ethylbenzene in nitrogen (red line) obtained by sweeping the laser injection current within the QCL_B tuning range at 235 mV peak-to-peak laser current modulation amplitude and 500 Torr.

selectivity allows for precise measurements by concentrating on the target gas while reducing the impact of other compounds, thus eliminating false readings. Additionally, high selectivity results in better sensitivity, enabling sensors to detect even lower concentrations or subtle changes in multi-component mixtures. Thereby, the potential spectral interferences caused by ethylbenzene on toluene and benzene detection, as well as the interference caused by methane and ethane on propane have been investigated. A comparative analysis of the QEPAS signals obtained in pure nitrogen, without the presence of BTEX or propane, with the signals obtained in the presence of toluene, benzene, and propane has been performed. Furthermore, the mixture of these gases has been analyzed to assess any potential alterations in the spectral features or the maximum strength of the QEPAS signal. This analysis aims at verifying whether the complexity of the gas mixture affects the radiation-to-sound conversion efficiency ε of the process, which is

a figure of merit describing how effective the energy relaxation of a target molecule is in a specific gas matrix at a given pressure, following a photoacoustic excitation characterized by a modulation frequency f.[22]

Both the working pressures and the modulation depths remain those optimized as discussed previously.

Figure 12(a) illustrates a comparison of the QEPAS signal obtained for 240 ppm of benzene, 150 ppm of ethylbenzene, and pure nitrogen, by employing the setup depicted in Fig. 3 with QCL_T as the light source. The result confirms that both benzene and ethylbenzene have no absorption features detectable within the current dynamic range of QCL_T. This was confirmed by evaluating the point-by-point difference among the three spectra, resulting in fluctuations lower than the 1-σ fluctuations of the QEPAS signal at any fixed current value. The weak background spectral structure visible in all three cases can be attributed
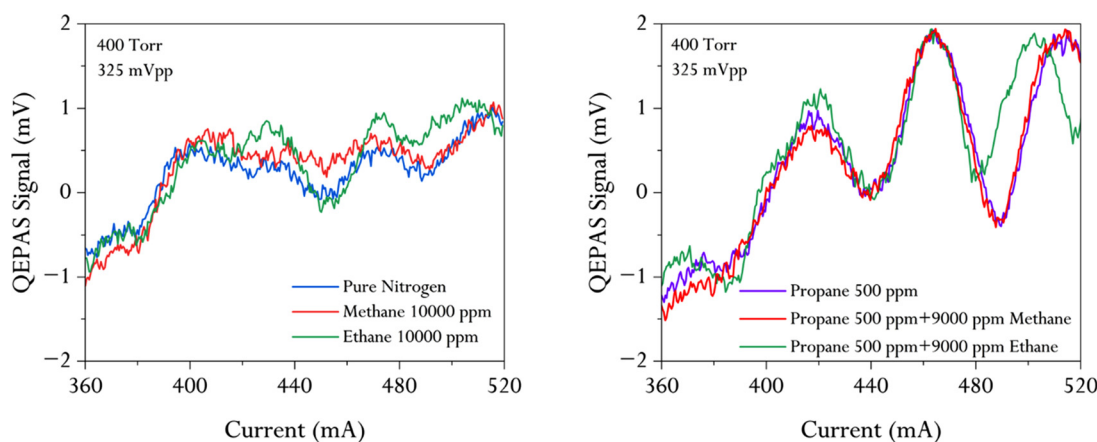
FIG. 13. (left panel) Comparison between the QEPAS signal obtained for 10 000 ppm of methane in nitrogen (red line), 10 000 ppm of ethane in nitrogen (green line), and pure nitrogen (blue line) obtained by sweeping the laser injection current within the QCL_P tuning range at 300 mV peak-to-peak laser current modulation amplitude and 400 Torr. (Right panel) Comparison of QEPAS signal for 500 ppm of propane in nitrogen (purple line) with two mixtures: 500 ppm of propane mixed with 9000 ppm of methane in nitrogen (red line) and 500 ppm of propane mixed with 9000 ppm of ethane in nitrogen (green line).

to the changes in the transmissivity of Ge optical windows at longer wavelengths.[47]

The further verification to carry out consists in evaluating whether toluene detection would be affected by the presence of benzene and ethylbenzene in terms of radiation-to-sound conversion efficiency, thus, in the form of matrix effect. Figure 12(b) compares the QEPAS spectral feature of toluene acquired in three different dilutions: 30 ppm of toluene in N_2, 30 ppm of toluene with 40 ppm of ethylbenzene in N_2, and 30 ppm of toluene with 192 ppm of benzene in N_2. The full overlap of the three spectra indicates that both the peak value and the shape of the feature is preserved, within the 1-σ fluctuations of the QEPAS signal for the strongest peak. Since the QEPAS signal is directly proportional to ε,[22] this result confirms that even a massive contamination from ethylbenzene and/or benzene in the mixture does not affect the efficiency of radiation-to-sound conversion in the toluene detection, eliminating the problem of the QEPAS signal dependence on matrix variations with respect to those two contaminants.

Figure 12(c) compares the QEPAS signal obtained with QCL_B for 10 ppm of benzene in N_2 with a gas mixture comprising 10 ppm of benzene combined with 68 ppm of toluene and 20 ppm of ethylbenzene in N_2. Here as well, both the shape of the spectral scans and the peak amplitude remain the same, indicating a negligible influence in the radiation-to-sound conversion efficiency.

Finally, the left panel in Fig. 13 reports the comparison between the QEPAS spectral scans obtained for a mixture of 10 000 ppm of methane in N_2 and a mixture of 10000 ppm of ethane, together with the acquisition in pure nitrogen. For this spectral configuration, QCL_P was employed in the experimental setup of Fig. 3. Slight differences among the spectral scans within the overall tuning range of QCL_P are hardly distinguishable, even exploring very high concentration ranges for the two analytes.

Furthermore, the right panel in Fig. 13 compares the QEPAS signals obtained for 500 ppm of propane in N_2 with two different gas mixtures. The first mixture comprises 500 ppm of propane combined with 9000 ppm of methane in N_2, while the second mixture consists of 500 ppm of propane combined with 9000 ppm of ethane in N_2. From

the right panel, it can be easily argued that there is a perfect correspondence between the QEPAS scan of propane in pure N_2 and the acquisition related to the mixture containing propane and methane. It is also clear that when ethane is present in the gas sample, some differences in terms of QEPAS spectrum shape arise with respect to the sample containing only propane, especially approaching the upper limit of the injection current span. This is due to a nonzero absorption of ethane within the investigated spectral range. Nevertheless, if the only central feature of propane peaked at 470 mA is considered, the three spectra tend to perfectly overlap in proximity to the peak value. This confirms one more time how important the identification of the most suitable modulation depth is, with the aim of selectively performing on-peak measurements without any kind of spectral/non spectral interference for propane, even in the presence of other lighter alkanes, which are normally expected at higher abundances in natural gas-like mixtures.

CONCLUSION AND PERSPECTIVES

Long wavelength spectroscopy is a still substantially unexplored research field that could allow the detection of VOCs with distinctive spectral fingerprints. Indeed, in the wavelength range between 10 and 20 μm, the absorption features of species like BTEXs or hydrocarbons can be very well separated with respect to the mid- and near-IR range, opening the way to their selective detection even in complex mixtures.

In this research manuscript, a QEPAS architecture for detection of two representative BTEXs such as benzene and toluene, together with propane, has been designed and demonstrated. Propane is the first hydrocarbon of the light alkanes without distinctive spectral features in the hydrocarbon window, i.e., 3–4 μm range, with respect to methane and ethane, while all the BTEXs show broad and overlapped absorption bands in the hydrocarbon window. The response of these three analytes to the photoacoustic excitation has been calibrated and characterized with respect to some of their most common interferents.

Response linearity and detection limits of 113 ppb, 3 ppb, and 3 ppm, respectively, have been demonstrated for toluene, benzene, and propane in pure nitrogen matrix at an integration time of 10 s. However, more importantly, a high level of selectivity with respect to

the composition variations of the gaseous matrix has been demonstrated for each of the three analytes considered. This result is very important because it has been obtained for a sensing system such as QEPAS, which is very robust and compact, but still based on an indirect technique and therefore subject to dependence on the gaseous matrix. Future research work will be dedicated to even more delicate spectroscopic scenarios, like discrimination and quantification of xylene isomers' concentration. The same spectral region will also be explored with alternative tuning fork-based spectroscopic approaches, like light-induced thermoelastic spectroscopy (LITES), exploiting the high absorbance of quartz at long wavelengths.

AUTHOR DECLARATIONS
Conflict of Interest

The authors have no conflicts to disclose.

Author Contributions

Kumar Kinjalk: Conceptualization (equal); Data curation (lead); Formal analysis (lead); Investigation (equal); Methodology (equal); Software (equal); Supervision (equal); Validation (equal); Visualization (equal); Writing – original draft (lead); Writing – review & editing (equal). **Francesco Paciolla:** Conceptualization (equal); Data curation (equal); Formal analysis (equal); Investigation (equal); Methodology (equal); Software (equal); Validation (equal); Visualization (equal); Writing – original draft (lead); Writing – review & editing (equal). **Bo Sun:** Data curation (equal); Formal analysis (equal); Investigation (equal); Software (equal); Validation (equal); Writing – review & editing (equal). **Andrea Zifarelli:** Conceptualization (equal); Data curation (equal); Formal analysis (equal); Software (equal); Supervision (equal); Validation (equal);

Writing – review & editing (equal). **Giansergio Menduni:** Conceptualization (equal); Data curation (equal); Formal analysis (equal); Investigation (equal); Methodology (equal); Software (equal); Supervision (equal); Validation (equal); Writing – review & editing (equal). **Marilena Giglio:** Conceptualization (equal); Data curation (equal); Formal analysis (equal); Investigation (equal); Methodology (equal); Software (equal); Supervision (equal); Validation (equal); Writing – review & editing (equal). **Hongpeng Wu:** Conceptualization (equal); Investigation (equal); Methodology (equal); Supervision (equal); Validation (equal); Writing – review & editing (equal). **Lei Dong:** Conceptualization (equal); Investigation (equal); Methodology (equal); Supervision (equal); Validation (equal); Writing – review & editing (equal). **Diba Ayache:** Conceptualization (equal); Formal analysis (equal); Investigation (equal); Methodology (equal); Writing – review & editing (equal). **Davide Pinto:** Formal analysis (equal); Investigation (equal); Writing – review & editing (equal). **Aurore Vicet:** Conceptualization (equal); Formal analysis (equal); Investigation (equal); Methodology (equal); Writing – review & editing (equal). **Alexei Baranov:** Conceptualization (equal); Investigation (equal); Methodology (equal); Resources (equal); Supervision (equal); Writing – review & editing (equal). **Pietro Patimisco:** Conceptualization (equal); Investigation (equal); Methodology (equal); Resources (equal); Supervision (equal); Writing – review & editing (equal). **Angelo Sampaolo:** Conceptualization (lead); Formal analysis (equal); Investigation (equal); Methodology (equal); Supervision (equal); Validation (equal); Visualization (equal); Writing – original draft (equal); Writing – review & editing (equal). **Vincenzo Spagnolo:** Conceptualization (equal); Writing – review & editing (equal).

DATA AVAILABILITY

The data that support the findings of this study are available from the corresponding authors upon reasonable request.

REFERENCES

[1] A. Trakoli, Occup. Med. **62**, 232 (2012).
[2] M. T. Smith, Annu. Rev. Public Health **31**, 133 (2010).
[3] A. N. Baghani, A. Sorooshian, M. Heydari, R. Sheikhi, S. Golbaz, Q. Ashournejad, M. Kermani, F. Golkhorshidi, A. Barkhordari, A. J. Jafari, M. Delikhoon, and A. Shahsavani, Environ. Pollut. **247**, 607 (2019).
[4] A. Garg, N. C. Gupta, and S. K. Tyagi, Environ. Claims J. **31**, 5 (2019).
[5] M. M. Greenberg, Environ. Res **72**, 1–7 (1997).
[6] B. Yu, Z. Yuan, Z. Yu, and F. Xue-song, Chem. Eng. J. **435**, 134825 (2022).
[7] Committee on Acute Exposure Guideline Levels, Committee on Toxicology, Board on Environmental Studies and Toxicology, Division on Earth and Life Studies, and National Research Council, *Acute Exposure Guideline Levels for Selected Airborne Chemicals* (National Academies Press, Washington, DC, 2012).
[8] F. S. Cikach and R. A. Dweik, Prog. Cardiovasc. Dis. **55**, 34 (2012).
[9] C. Lourenço and C. Turner, Metabolites **4**, 465 (2014).
[10] A. Sharma, R. Kumar, and P. Varadwaj, Mol. Diagn. Ther. **27**, 321 (2023).
[11] D. Poli, P. Carbognani, M. Corradi, M. Goldoni, O. Acampa, B. Balbi, L. Bianchi, M. Rusca, and A. Mutti, Respir. Res. **6**, 71 (2005).
[12] F. W. Karasek and R. E. Clement, in *Basic Gas Chromatography—Mass Spectrometry* (Elsevier, 1988), pp. 79–159.
[13] D. O. Sparkman, Z. E. Penton, and F. G. Kitson, in *Gas Chromatography and Mass Spectrometry: A Practical Guide* (Elsevier, 2011), pp. xv–xvii.
[14] F. Opekar and K. Štulík, *In Encyclopedia of Analytical Chemistry* (John Wiley & Sons, Ltd, Chichester, UK, 2009).

[15]M. J. Madou and S. R. Morrison, *Chemical Sensing with Solid State Devices* (Elsevier, 1989).

[16]J. Hodgkinson and R. P. Tatam, Meas. Sci. Technol. **24**, 012004 (2013).

[17]K. Ruxton, A. L. Chakraborty, W. Johnstone, M. Lengden, G. Stewart, and K. Duffin, Sens. Actuators, B **150**, 367 (2010).

[18]J. Cousin, W. Chen, D. Bigourd, M. Fourmentin, and S. Kassi, Appl. Phys. B **97**, 919 (2009).

[19]J. Waschull, B. Sumpf, Y. Heiner, and H.-D. Kronfeldt, Infrared Phys. Technol. **37**, 193 (1996).

[20]M. Mhanna, M. Sy, A. Arfaj, J. Llamas, and A. Farooq, Opt. Lett. **47**(13), 3247–3250 (2022).

[21]I. E. Gordon, L. S. Rothman, R. J. Hargreaves, R. Hashemi, E. V. Karlovets, F. M. Skinner, E. K. Conway, C. Hill, R. V. Kochanov, Y. Tan, P. Wcisło, A. A. Finenko, K. Nelson, P. F. Bernath, M. Birk, V. Boudon, A. Campargue, K. V. Chance, A. Coustenis, B. J. Drouin, J. M. Flaud, R. R. Gamache, J. T. Hodges, D. Jacquemart, E. J. Mlawer, A. V. Nikitin, V. I. Perevalov, M. Rotger, J. Tennyson, G. C. Toon, H. Tran, V. G. Tyuterev, E. M. Adkins, A. Baker, A. Barbe, E. Canè, A. G. Császár, A. Dudaryonok, O. Egorov, A. J. Fleisher, H. Fleurbaey, A. Foltynowicz, T. Furtenbacher, J. J. Harrison, J. M. Hartmann, V. M. Horneman, X. Huang, T. Karman, J. Karns, S. Kassi, I. Kleiner, V. Kofman, F. Kwabia-Tchana, N. N. Lavrentieva, T. J. Lee, D. A. Long, A. A. Lukashevskaya, O. M. Lyulin, V. Y. Makhnev, W. Matt, S. T. Massie, M. Melosso, S. N. Mikhailenko, D. Mondelain, H. S. P. Müller, O. V. Naumenko, A. Perrin, O. L. Polyansky, E. Raddaoui, P. L. Raston, Z. D. Reed, M. Rey, C. Richard, R. Tóbiás, I. Sadiek, D. W. Schwenke, E. Starikova, K. Sung, F. Tamassia, S. A. Tashkun, J. Vander Auwera, I. A. Vasilenko, A. A. Vigasin, G. L. Villanueva, B. Vispoel, G. Wagner, A. Yachmenev, and S. N. Yurchenko, J. Quant. Spectrosc. Radiat. Transfer **277**, 107949 (2022).

[22]A. Sampaolo, P. Patimisco, M. Giglio, A. Zifarelli, H. Wu, L. Dong, and V. Spagnolo, Anal. Chim. Acta **1202**, 338894 (2022).

[23]E. Benveniste, A. Vasanelli, A. Delteil, J. Devenson, R. Teissier, A. Baranov, A. M. Andrews, G. Strasser, I. Sagnes, and C. Sirtori, Appl. Phys. Lett. **93**, 131108 (2008).

[24]H. Nguyen Van, Z. Loghmari, H. Philip, M. Bahriz, A. Baranov, and R. Teissier, Photonics **6**, 31 (2019).

[25]M. Carras, M. Garcia, X. Marcadet, O. Parillaud, A. De Rossi, and S. Bansropun, Appl. Phys. Lett. **93**, 11109 (2008).

[26]Y. Jin, F. Sun, J. Li, C. S. Tan, K. H. Tan, S. Wicaksono, C. Sirtori, S. F. Yoon, and Q. J. Wang, Opt. Express **31**, 27543 (2023).

[27]S. Lin, J. Chang, J. Sun, and P. Xu, Front. Phys. **10**, 853966 (2022).

[28]S. Brown, Chem. Rev. **103**, 5219 (2003).

[29]VIGO Photonics, see https://Vigophotonics.Com/Product/Pci-4te-14/ for "HgCdTe (MCT) Photoconductive Detector PCI-4TE-14."

[30]K. F. Mak, L. Ju, F. Wang, and T. F. Heinz, Solid State Commun. **152**, 1341 (2012).

[31]C.-H. Liu, Y.-C. Chang, T. B. Norris, and Z. Zhong, Nat. Nanotechnol. **9**, 273 (2014).

[32]T. Wei, A. Zifarelli, S. Dello Russo, H. Wu, G. Menduni, P. Patimisco, A. Sampaolo, V. Spagnolo, and L. Dong, Appl. Phys. Rev. **8**, 041409 (2021).

[33]D. Ayache, W. Trzpil, R. Rousseau, K. Kinjalk, R. Teissier, A. N. Baranov, M. Bahriz, and A. Vicet, Opt. Express **30**, 5531 (2022).

[34]J. Karhu, H. Philip, A. Baranov, R. Teissier, and T. Hieta, Opt. Lett. **45**, 5962 (2020).

[35]P. Luo, J. Harrist, G. Menduni, R. Mesdour, N. StMichel, and A. Sampaolo, ACS Omega **7**, 3395 (2022).

[36]A. Sampaolo, S. Csutak, P. Patimisco, M. Giglio, G. Menduni, V. Passaro, F. K. Tittel, M. Deffenbaugh, and V. Spagnolo, Sens. Actuators, B **282**, 952 (2019).

[37]A. Zifarelli, M. Giglio, G. Menduni, A. Sampaolo, P. Patimisco, V. M. N. Passaro, H. Wu, L. Dong, and V. Spagnolo, Anal. Chem. **92**, 11035 (2020).

[38]G. Gassler, B. Reißenauer, and W. Hüttner, Z. Naturforsch., A **44**, 316 (1989).

[39]K. Kinjalk, D. A. Díaz-Thomas, Z. Loghmari, M. Bahriz, R. Teissier, and A. N. Baranov, Photonics **9**, 747 (2022).

[40]Thorlabs, see https://www.Thorlabs.Com/Thorproduct.Cfm?Partnumber=TH100PT for "TH100PT 100 Ω Platinum Resistance Temperature Detector."

[41]P. M. Chu, F. R. Guenther, G. C. Rhoderick, and W. J. Lafferty, J. Res. Natl. Inst. Stand. Technol. **104**, 59 (1999).

[42]M. Margoshes and V. A. Fassel, Spectrochim. Acta **7**, 14 (1955).

[43]P. Patimisco, A. Sampaolo, M. Giglio, S. dello Russo, V. Mackowiak, H. Rossmadl, A. Cable, F. K. Tittel, and V. Spagnolo, Opt. Express **27**, 1401 (2019).

[44]S. Dello Russo, A. Sampaolo, P. Patimisco, G. Menduni, M. Giglio, C. Hoelzl, V. M. N. Passaro, H. Wu, L. Dong, and V. Spagnolo, Photoacoustics **21**, 100227 (2021).

[45]P. Patimisco, A. Sampaolo, H. Zheng, L. Dong, F. K. Tittel, and V. Spagnolo, Adv. Phys. X **2**, 169 (2016).

[46]P. Patimisco, A. Sampaolo, Y. Bidaux, A. Bismuto, M. Scott, J. Jiang, A. Muller, J. Faist, F. K. Tittel, and V. Spagnolo, Opt. Express **24**, 25943 (2016).

[47]See https://www.Thorlabs.Com/Newgrouppage9.Cfm?Objectgroup_id=3980&gclid=CjwKCAjwvfmoBhAwEiwAG2tqzPVYZtwLMNdhxMOQ46kA_wMauMH3V1h2Ws_cdSCHxjv0SG7LYtVgAhoC0HcQAvD_BwE for "THORLABS—Germanium Windows."

06 December 2024 08:15:39